Nuclear deformation in excited Pb isotopes from giant dipole γ-ray–fission angular correlations

R. Butsch, M. Thoennessen, D. R. Chakrabarty,* M. G. Herman, and P. Paul
Department of Physics, State University of New York at Stony Brook, Stony Brook, New York 11794
(Received 31 October 1989)

Angular correlations between γ rays and fission fragments were measured in the reaction $^{19}F+^{181}Ta$ at 105 and 141 MeV bombarding energy. These correlations are used to extract the probability of giant dipole resonance γ-ray emission relative to the spin axis of the compound system which gives direct information about the projection quantum numbers of the split giant dipole resonance components in a deformed nucleus. Large anisotropies observed in the γ-ray energy region of the compound nucleus giant dipole resonance demonstrate unambiguously a deformed shape of the ^{200}Pb compound system at excitation energies of 69.5 and 102.4 MeV. The singles and fission-coincidence γ-ray spectra are fitted consistently in terms of the statistical γ-ray decay of the compound system and excited fission fragments. The giant dipole resonance parameters of these fits are then used to compute the γ-ray angular distribution with respect to the compound nucleus spin axis for prolate and oblate shapes. At 69.5 MeV the γ-ray anisotropy relative to the compound nucleus spin axis is well described by a prolate shape with a deformation $\beta=0.43$ in general agreement with theoretical predictions of a superdeformed shape in ^{200}Pb. However, the large observed deformation survives to much higher temperatures than predicted. At 102.4 MeV the data require a reduction of the fission probability in the very early decay steps of the compound system. At this excitation energy the extraction of the shape of the ^{200}Pb nucleus is ambiguous, allowing both a collective prolate as well as a noncollective oblate shape.

I. INTRODUCTION

The deformations of hot rotating nuclei have now been investigated in a number of cases by studying the decay of the giant dipole resonance (GDR) built on highly excited states that are produced in heavy-ion fusion reactions.[1] In these cases, the deformation is obtained from the splitting of the giant dipole strength function. One goal of these studies is to observe the predicted general shape transition[2,3] from collective prolate to noncollective oblate at nuclear temperatures between 1 and 2 MeV. In principle, the GDR strength function contains information about the prolate or oblate character of the nuclear shape, but it has proved difficult to extract this information unambiguously from singles γ-ray spectra alone.[4] Thus, differentiation between collective prolate, collective oblate (nuclear symmetry axis perpendicular to rotation axis), or noncollective oblate (nuclear symmetry axis parallel to rotation axis) shapes requires an additional measurement of the γ-ray angular distribution relative to a suitable quantization axis. While the γ-ray angular distribution for giant dipole decay of highly excited nuclei is nearly isotropic for a spherical nucleus,[1,5] a deformation causes an anisotropy that depends on the quantum numbers of the GDR vibrations in the body fixed coordinate system of the nucleus. This anisotropy is more pronounced for γ-ray angular distributions measured with respect to the spin axis of the compound nucleus (CN) than with respect to the beam axis, since the latter measurement averages over all possible CN spin directions. This averaging process makes it difficult to extract shape information directly from γ-ray angular distribution measurements relative to the beam axis.[6–9] On the other side, low-energy γ-ray transitions allow the determination of the CN spin axis. Results on high-energy γ rays obtained by this method were interpreted as a spin dependent shift of the centroid position of the GDR,[10] and as an indication (although statistically barely significant) of nonstatistical γ-ray emission[11] in an energy region close to the GDR. A different approach to fix the CN spin axis is available in heavy nuclei, where fission is a strong decay channel. Here, the CN spin direction may be determined directly from the direction of the fission fragments. In the classical limit the spin points perpendicular to the reaction plane defined by the fission fragments.

It is the purpose of this paper to present measurements of γ-ray angular distributions with respect to the CN spin axis via a γ-ray-fission angular correlation and to derive the equations of the correlation in terms of GDR and nuclear shape parameters. We apply this procedure to neutron deficient Pb isotopes where the previous observation[12] of a split GDR indicates a large deformation of $\beta\approx0.3$ at excitation energies from 66 to 103 MeV obtained from γ-ray singles measurements. This deformation agrees with the theoretical prediction[13,14] of a superdeformed prolate shape in $^{196-202}Pb$ above a spin of about $20\hbar$. A recent analysis of the GDR line shape observed in the $^{19}F+^{181}Ta$ fusion reaction indicates indeed an onset of the superdeformation between $13\hbar$ and $17\hbar$.[15] This experiment studies this deformation in more detail by detecting GDR γ rays in coincidence with fission fragments. Such a coincidence experiment gates on the very early decay steps of the compound system. For low bombarding energies around 100 MeV, fission of the Pb nuclei occurs only in the high partial waves ($J \approx 30\hbar - 40\hbar$); therefore, a fission-coincidence experiment was performed at 105 MeV which selects preferentially GDR γ rays emitted from the CN in its superdeformed shape. Calculations predict[14] that the superdeformed minimum should be washed out at a temperature $T \approx 1.3$ MeV and spin $J \approx 40\hbar$. To test the influence of temperature and angular momentum, a coincidence measurement was also performed at the higher bombarding energy of 141 MeV which produces a temperature of ≈ 1.5 MeV for the CN-GDR basis states, and an average angular momentum of $\approx 50\hbar$.

II. THE EXPERIMENT

A 0.8 mg/cm^2 thick self-supporting ^{181}Ta target was bombarded with 105 and 141 MeV ^{19}F ions from the Stony Brook Tandem-Linac producing the compound nucleus ^{200}Pb. Typical beam currents were 10 particle nA. The beam was pulsed with a repetition period of 106 ns. γ rays were detected in a 25.4$\times$38.1 cm cylindrical NaI detector, with its front face located 50 cm from the target, 90° to the beam as depicted in Fig. 1(a). Neutron, cosmic ray, and pileup rejection as well as the energy calibration for the NaI detector was achieved following the prescription detailed elsewhere.[5,16] Fission fragments were detected in four silicon surface barrier detectors. Each (100 μm thick, area of 300 mm^2) was located 6 cm from the target. An aperture limited the solid angle for each fission detector to 60 msr, or an angular range $\Delta\Theta = \pm 8°$. The fragment detectors were placed in a plane perpendicular to the beam axis and at 90° to each other in such a way that one pair of fission detectors ($F2$ and $F4$) was aligned with the axis of the NaI detector while the second pair ($F1$ and $F3$) was perpendicular to it [Fig. 1(b)]. In this geometry, a γ ray detected in coincidence with $F1$ or $F3$ ($F2$ or $F4$) was emitted parallel (perpendicular) to the CN spin axis (with some corrections discussed later). The reaction kinematics in this experiment are such that only one fragment of each fission event is detected, and the 180° partners serve only to double the solid angle. The target was turned 45° to the fission detector plane and 45° to the beam axis, increasing the target thickness for the beam to 1.6 mg/cm^2. Taking into account the energy loss to the middle of the target, the mean excitation energies for these experiments were 69.5 and 102.4 MeV. Fission fragments were unambiguously identified by measuring their energy and time-of-flight (with respect to the radio frequency of the accelerator; see Fig. 2). The (lower-energy) fission fragments are clearly separated in time from the (higher-energy) quasi-elastic scattered projectiles. Part of the time difference can be attributed to the larger plasma delay for fission fragments in silicon detectors[17] with respect to scattered ^{19}F ions.

Any of three trigger conditions defined a valid event: a coincidence between the NaI detector and any of the fission detectors, a scaled down fission singles event, or a valid γ-ray multiplicity coincidence with the NaI detector. The γ-ray multiplicity gated ("singles") γ-ray spectra were recorded using ten 7.6$\times$10.2 cm NaI detectors as a multiplicity filter [Fig. 1(a)].[5] The fold N of the multiplicity filter, required to select fusion events, was set to $N > 1$. We present here singles data for 141 and 105 MeV, where the latter data set was previously published.[12] Scaled down fission singles events were recorded simultaneously to normalize the γ-ray coincidence spectra obtained with the four fission detectors to each other.

In the off-line analysis two-dimensional time-of-flight energy windows were used to gate on the fission fragments. A time-of-flight window on the NaI detector selected prompt γ-ray events, with only a small subtraction for thermal neutron background required. After normalizing every coincidence γ-ray spectrum to its respective fission-singles yield, the γ-ray spectra resulting from coincidences with $F1$ and $F3$ (or $F2$ and $F4$) were summed to increase statistics. The ratios of the coincidence γ-ray energy spectra, $F1/F3$ and $F2/F4$ were unity, within statistical uncertainty, justifying the summing procedure. The final product of the correlation experiment is the ratio of γ ray yields with respect to the CN spin axis at 0° and 90°, $W(0°,E_\gamma)/W(90°,E_\gamma)$, as a function of γ-ray energy E_γ, which is obtained from the ratio of the summed γ-ray spectra in coincidence with the fission detectors, i.e., $(F1+F3)/(F2+F4)$.

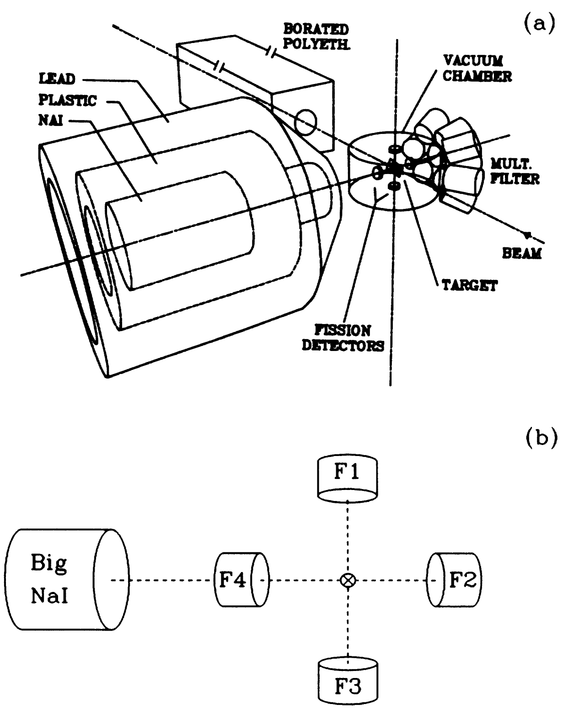

FIG. 1. (a) Experimental setup for the γ-ray-fission correlation experiment. (b) The lower part shows the geometry of the four fission detectors $F1$-$F4$ in more detail with the beam axis perpendicular to the picture plane.

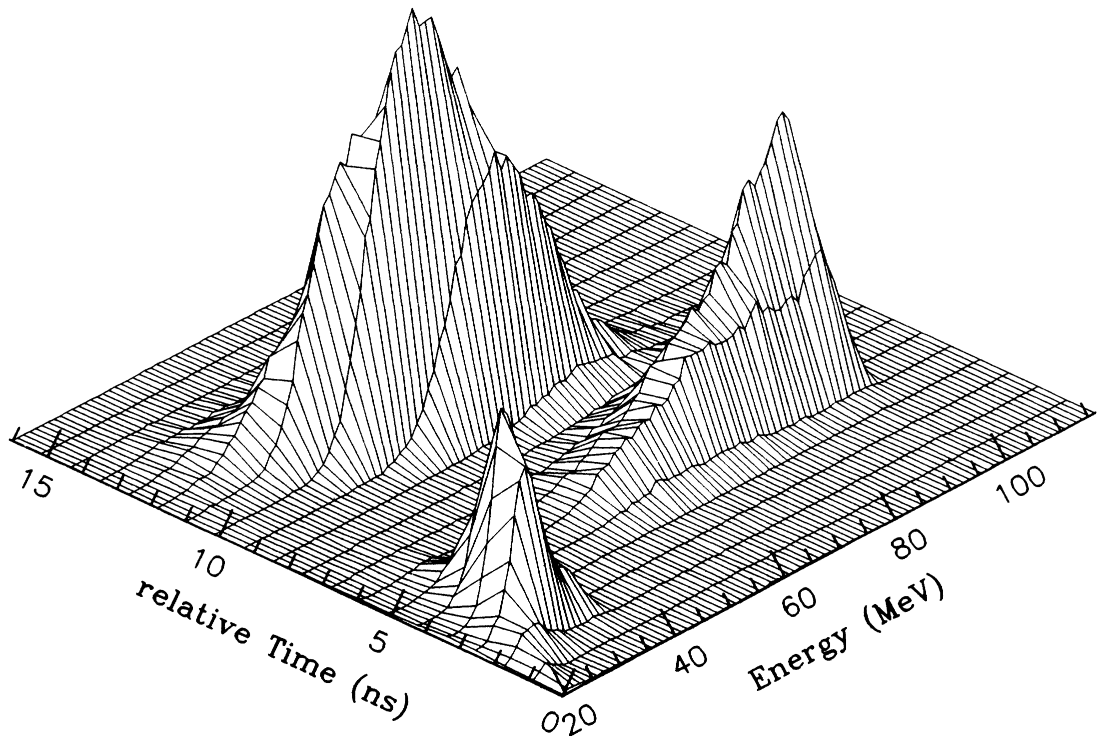

FIG. 2. Energy versus time-of-flight (TOF) spectrum for 105 MeV $^{19}F + ^{181}Ta$ measured with one fission detector. Time and energy axes are not calibrated absolutely.

III. GIANT DIPOLE γ-RAY-FISSION ANGULAR CORRELATIONS

In this section we derive the γ-ray angular distribution for giant dipole γ-ray decay with respect to the CN spin axis, which is defined experimentally by a correlation measurement with fission fragments. We present this angular distribution in the high spin limit which is a good approximation for heavy-ion fusion reactions.

In an axially symmetric deformed nucleus the GDR energies are split into dipole vibrations parallel and perpendicular to the nuclear symmetry axis. Taking this axis as the quantization axis the γ-ray angular distribution for dipole radiation in the body fixed system is a combination of $\eta = m_i - m_f = 0$ parallel vibrations and $\eta = \pm 1$ perpendicular vibrations. Here, η is the projection of the transition angular momentum ($L=1$) associated with the GDR vibration on the body fixed symmetry axis with m_i and m_f the magnetic substates in the initial and final nuclear states. The angular distributions for these vibrations are given by[18]

$$\eta=0: \quad W^{\parallel}(\theta') = 1 - P_2(\cos\theta') ,$$

$$\eta=\pm 1: \quad W^{\perp}(\theta') = 1 + \tfrac{1}{2}P_2(\cos\theta') ,$$

where θ' is the angle between the γ ray and the intrinsic (fixed) symmetry axis and $P_2(\cos\theta')$ represents a Legendre polynomial. The superscripts $\parallel$ and $\perp$ will refer throughout this paper to vibrations parallel and perpendicular to the nuclear symmetry axis, respectively.

In the case of a deformed compound nucleus rotating collectively, the nuclear symmetry axis is perpendicular to the CN spin axis. The reaction plane, defined by the fission fragments and the beam direction, fixes the CN spin axis perpendicular to the plane. Since the nuclear symmetry axis lies in the reaction plane, an angular distribution measurement with respect to the CN spin axis requires an averaging of $W(\theta')$ over all possible angles of the symmetry axis in this plane. This yields

$$\eta=0: \quad W^{\parallel}(\theta) = 1 + \tfrac{1}{2}P_2(\cos\theta) ,$$

$$\eta=\pm 1: \quad W^{\perp}(\theta) = 1 - \tfrac{1}{4}P_2(\cos\theta) .$$

The γ-ray emission angle θ is now measured with respect to the CN spin axis.

In the case of a noncollective rotational nucleus the intrinsic symmetry axis is parallel to the spin axis. Since the latter is fixed by the fission fragments, no transformation of the quantization axis has to be performed. Therefore, the angular distribution of $E1$ γ rays with respect to the CN spin axis is given by

$$\eta=0: \quad W^{\parallel}(\theta) = 1 - P_2(\cos\theta) ,$$

$$\eta=\pm 1: \quad W^{\perp}(\theta) = 1 + \tfrac{1}{2}P_2(\cos\theta) .$$

We note that the a_2 coefficients for angular distributions with respect to the spin axis have opposite signs and are twice as large as those obtained with respect to the beam axis, because the experiment does not average over CN spin directions.

These a_2 coefficients, however, represent a maximum value since the axis of collective rotation may be disoriented due to thermal effects which uncouples single particles from the collective rotation. This will not happen for noncollective shapes. Here, the symmetry axis is always parallel to the total angular momentum, which, by definition, is entirely due to single-particle alignment. Therefore, in the following, a deorientation of the nuclear shape relative to the CN spin axis will be considered only for collective shapes. It was included in the formalism in the following way.

For a collective prolate deformed nucleus the a_2 coefficient with respect to the spin axis for a GDR vibration parallel to the symmetry axis is of pure $\Delta J=\pm 1$ nature. A deorientation of the symmetry axis with respect to the spin axis will give rise to $\Delta J=0$ admixtures. Thus, the a_2 coefficient is given by a weighted sum of each contribution

$$a_2^{\parallel}=a_2^{\Delta J=\pm 1}\sin^2\psi_{\mathrm{eq}}+a_2^{\Delta J=0}\cos^2\psi_{\mathrm{eq}} ,$$

where ψ_{eq} relates the axis of symmetry to the nuclear spin axis at equilibrium deformation.

For vibrations perpendicular to the symmetry axis one has to bear in mind that a deorientation does not affect a vibration that is perpendicular to the symmetry axis and perpendicular to the spin axis. Taking this into consideration the a_2 coefficient with respect to the spin axis for vibrations perpendicular to the symmetry axis reads

$$a_2^{\perp}=\tfrac{1}{2}[a_2^{\Delta J=0}\sin^2\psi_{\mathrm{eq}}+a_2^{\Delta J=\pm 1}(1+\cos^2\psi_{\mathrm{eq}})] .$$

Using

$$\cos^2\psi_{\mathrm{eq}}=k_{\mathrm{eq}}/J(J+1) ,$$

with k_{eq} the projection of spin J onto the symmetry axis at equilibrium deformation, and values for the a_2 coefficients with respect to the spin axis in the high spin limit ($a_2^{\Delta J=\pm 1}=\frac{1}{2}$, $a_2^{\Delta J=0}=-1$) one obtains

$$W_J(\theta)=1+a_2Q_2P_2(\cos\theta)\left[1-\sum_{k_{\mathrm{eq}}}\frac{3k_{\mathrm{eq}}^2}{J(J+1)}P_{\mathrm{eq}}(k_{\mathrm{eq}})\right] ,$$

with $a_2=\frac{1}{2}$ $(-\frac{1}{4})$ for parallel (perpendicular) vibrations and collective rotation. As noted before, for noncollective oblate shapes, the angular distribution remains

$$W_J(\theta)=1+a_2Q_2P_2(\cos\theta)$$

with $a_2=-1$ $(+\frac{1}{2})$ for parallel (perpendicular) vibrations. Geometric attenuation coefficients[19] for the NaI detector are denoted by Q_2, with $Q_2(E_\gamma)\geq 0.97$ for our geometry. $P_{\mathrm{eq}}(k_{\mathrm{eq}})$ describes a Gaussian distribution (normalized to 1) of k_{eq} values at equilibrium deformation with a standard deviation $K_{0,\mathrm{eq}}$ given by $K_{0,\mathrm{eq}}^2=T_{\mathrm{eq}}\mathcal{J}_{\mathrm{eff,eq}}/\hbar^2$ with T_{eq} the temperature and $\mathcal{J}_{\mathrm{eff,eq}}$ the effective moment of inertia (see further discussion in Sec. IV B).

In the next step, modifications in the translation of the spin axis into the direction of the fission fragments have to be considered. It is well known that a statistical tilt of the nuclear symmetry axis with respect to the CN spin axis must be included when the system goes over the fission saddle point.[20] This tilt may be described by a normalized Gaussian distribution of k values at the saddle point, $P_s(k_s)$, with standard deviation $K_{0,s}^2=T_s\mathcal{J}_{\mathrm{eff},s}/\hbar^2$, with the temperature and effective moment of inertia determined at the saddle point. Since the GDR γ ray is detected in coincidence with the fission fragment, each k_{eq} projection at equilibrium deformation is affected by the saddle-point distribution, and hence, both distributions have to be folded:

$$W_J(\theta)=1+a_2Q_2P_2(\cos\theta)\left[1-\sum_{k_{\mathrm{eq}}}\sum_{k_s}\frac{3(k_{\mathrm{eq}}-k_s)^2}{J(J+1)}P_{\mathrm{eq}}(k_{\mathrm{eq}}-k_s)P_s(k_s)\right] .$$

In the following, it is assumed that the k distribution, i.e., the spin axis, at the saddle point is frozen when the system moves to scission.

It now remains to relate the angle θ between the spin axis at the saddle point and the γ ray to the experimental configuration, i.e., to the angle φ between the NaI detector and an ideal axis exactly perpendicular to the reaction plane that is defined by the fission fragment detectors. Figure 3 illustrates this situation for the special case of $\varphi=90°$. There are two possible spin orientations (angles θ_1 and θ_2) having the same k_s projection and which cannot be distinguished. The angle ψ_s is defined as $\cos^2\psi_s=k_s^2/J(J+1)$. In the general situation ($\varphi\neq 0°,\neq 90°$) one has to average over both spin directions $\theta_1=\varphi+\psi_s-90°$ and $\theta_2=\varphi-\psi_s+90°$ for a given k_s, yielding

$$W_J(\varphi)=1+a_2^*Q_2\left[P_2(\cos\varphi)-\tfrac{1}{2}(\cos^2\varphi-\sin^2\varphi)\sum_{k_s}\frac{3k_s^2}{J(J+1)}P_s(k_s)\right] \tag{1}$$

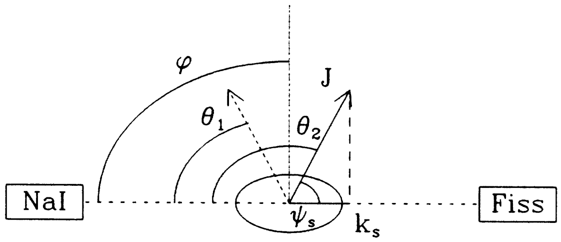

FIG. 3. Schematic illustration of the tilting of the nuclear symmetry axis of the compound system as it moves over the fission saddle point. The various angles are explained in the text.

with the abbreviation

$$a_2^* = a_2 \left[1 - \sum_{k_{eq}} \sum_{k_s} \frac{3(k_{eq}-k_s)^2}{J(J+1)} P_{eq}(k_{eq}-k_s) P_s(k_s) \right]$$

For our geometry, the angle $\varphi = 90°$ ($\varphi = 0°$) will then lead to angular distributions with the GDR γ-ray emitted perpendicular (parallel) to the CN spin axis including the "k wobbling" at the saddle point. The influence of the finite opening angle of the fission detector can be included by adjusting the width of the k distribution at the saddle point (see Sec. IV B).

Finally, after summing over the fission part of the fusion spin distribution in the entrance channel, σ_J^f, we obtain

$$W(\varphi) = \frac{\sum_J \sigma_J^f W_J(\varphi)}{\sum_J \sigma_J^f} . \tag{2}$$

With the assumption of a two-component Lorentzian for the split CN-GDR strength function the energy dependent ratio of the γ-ray angular distribution at $\varphi = 0°$ and $\varphi = 90°$ with respect to the spin is given by

$$\frac{W(0°,E_\gamma)}{W(90°,E_\gamma)} = \frac{F^{\parallel}(E_\gamma)W^{\parallel}(0°)+F^{\perp}(E_\gamma)W^{\perp}(0°)}{F^{\parallel}(E_\gamma)W^{\parallel}(90°)+F^{\perp}(E_\gamma)W^{\perp}(90°)} , \tag{3}$$

where the strength functions for the dipole vibrational modes for an axially symmetric nucleus are defined by

$$F^{\parallel}(E_\gamma) = S^{\parallel} \frac{\Gamma^{\parallel} E_\gamma^4}{(E_\gamma^2 - E^{\parallel 2})^2 + (\Gamma^{\parallel} E_\gamma)^2}$$

with $S^{\parallel} = \frac{1}{3}$, and similarly for $F^{\perp}$ with $S^{\perp} = \frac{2}{3}$. Here the GDR parameters for a vibration parallel to the intrinsic symmetry axis are $E^{\parallel}$ and $\Gamma^{\parallel}$, those for a perpendicular vibration are $E^{\perp}$ and $\Gamma^{\perp}$. For a prolate deformed nucleus the superscript $\parallel$ ($\perp$) refers to the lower (higher) resonance parameters, whereas for oblate deformed nuclei $\parallel$ ($\perp$) refers to the higher (lower) resonance parameters.

Figure 4 shows the anisotropy $W(0°,E_\gamma)/W(90°,E_\gamma)$ for a CN giant dipole γ-ray decay calculated with Eq. (3) for various shapes of the compound nucleus ^{200}Pb (neglecting at this point attenuation effects at equilibrium deformation). Clearly, the energy dependent anisotropy readily differentiates between prolate (solid curve) and oblate (short-dashed curve) nuclei rotating collectively, but it is more difficult to distinguish between the collective prolate and noncollective oblate (long-dashed curve) shape.

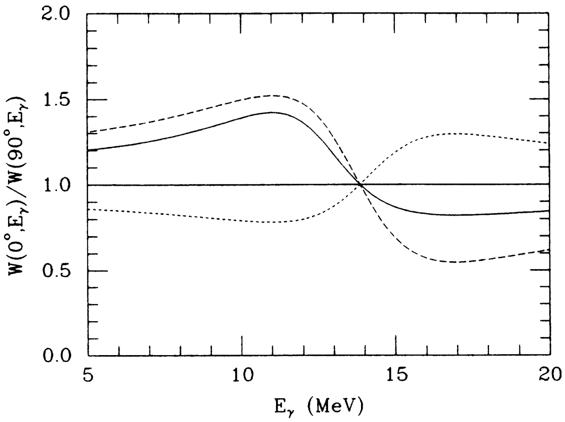

FIG. 4. Calculated anisotropy of compound nucleus γ rays for giant dipole transitions for different types of deformations (see the text), assuming a two component GDR with $E_{low} = 11.9$ MeV, $\Gamma_{low} = 3.8$ MeV, $E_{high} = 15.4$ MeV, $\Gamma_{high} = 5.3$ MeV, and $K_{0,s} = 12$. Note, that these curves correspond to the same energy splitting and therefore to different deformation values for prolate/oblate shapes [producing $W(0°,E_\gamma)/W(90°,E_\gamma) = 1$ at the same γ-ray energy].

Finally, we discuss several modifications which have to be applied to Eq. (3) before it can be compared to experiment.

(a) Equation (3) applies only to those γ rays that are emitted from the CN before fission ("prefission"), whereas in the coincidence experiment prefission γ rays as well as γ rays emitted from the excited fission fragments ("postfission") are observed. The contribution of the postfission γ rays to the γ-ray spectrum was obtained by calculating the prefission and postfission γ-ray cross sections, $\sigma_{\rm Pre}(E_\gamma)$ and $\sigma_{\rm Post}(E_\gamma)$, with a modified version of the statistical model code CASCADE as described in the next section.

(b) Post fission γ rays detected in the NaI detector in coincidence with the left ($F2$) and right ($F4$) fission detectors are Doppler shifted. Since the experiment cannot distinguish between prefission and postfission γ rays we apply the Doppler correction to the calculations. Therefore, Doppler-shifted γ-ray spectra $\sigma_{\rm Post}^{\rm Dopp}(E_\gamma)$ were calculated from $\sigma_{\rm Post}(E_\gamma)$. Assuming symmetric fission of the CN the recoil velocity v_f of the fragments at 90° relative to the beam axis in the laboratory system is $\beta_f = v_f/c = 0.038$. The postfission γ ray can be emitted either from the detected fragment or from the nonobserved complementary fragment, the latter having the same Doppler-shift projection onto the NaI axis (for symmetric fission) but with opposite sign. Therefore, the final Doppler corrected postfission γ-ray spectrum is given by an average over positive (Dopp+) and negative (Dopp−)

Doppler shifts. (As it is pointed out in the Appendix, a fission fragment mass distribution has been included in the analysis. The influence of different fission fragment masses on the Doppler-shift correction has been investigated and it has been found to be negligible. This is because the Doppler-shift correction procedure must average between the observed lighter fragment/nonobserved heavier fragment, and the reverse case.)

(c) Little is known about the angular distribution of high-energy postfission γ rays emitted from highly excited fission fragments produced in heavy-ion reactions. As will be discussed in Sec. IV B, nonisotropic γ-ray emission from deformed fission fragments will be considered. We assume collective prolate shapes for the fission fragments with a GDR γ-ray angular distribution pattern $W_f(\theta)=1+a_2P_2(\cos\theta)$. To simulate the effect of dealignment of the fragment spin orientation caused by internal excitation of angular momentum bearing modes[21] that add randomly to the spin distribution in the fission fragments, we use a Gaussian distribution $P_f(k_f)$ of k_f values (projection of J onto the symmetry axis of the fragment) with a standard deviation K_0^{frag}. This leads to the same expression as Eq. (1), with these exceptions: (i) a_2^* in Eq. (1) has to be replaced by the normal a_2 coefficient, and (ii) $P_s(k_s)$ has to be replaced by $P_f(k_f)$. This procedure assumes that part of the fragment spin is still aligned so that the angle φ also describes the angle between the postfission γ ray and the fragment spin direction parallel to the CN spin axis. To calculate the equivalent part of Eq. (2) for fission fragments we apply the procedure outlined in the Appendix for calculating the spin distribution in the fragments that turn out to be very narrow ("spin focusing effect").[21]

With these modifications Eq. (3) becomes

$$\frac{W(0°,E_\gamma)}{W(90°,E_\gamma)}=\frac{\sigma_{\text{Pre}}(E_\gamma)W_{\text{CN}}(0°,E_\gamma)+\sigma_{\text{Post}}(E_\gamma)W_f(0°,E_\gamma)}{\sigma_{\text{Pre}}(E_\gamma)W_{\text{CN}}(90°,E_\gamma)+\frac{1}{2}[\sigma_{\text{Post}}^{\text{Dopp}+}(E_\gamma)+\sigma_{\text{Post}}^{\text{Dopp}-}(E_\gamma)]W_f(90°,E_\gamma)}\,, \tag{4}$$

with

$$W_i(\varphi,E_\gamma)=\frac{F_i^{\parallel}(E_\gamma)}{F_i^{\parallel}(E_\gamma)+F_i^{\perp}(E_\gamma)}W_i^{\parallel}(\varphi)+\frac{F_i^{\perp}(E_\gamma)}{F_i^{\parallel}(E_\gamma)+F_i^{\perp}(E_\gamma)}W_i^{\perp}(\varphi)\ .$$

where the index i represents either the compound nucleus (CN) or the fission part (f) of the angular distribution of Eq. (2).

We note that the CN and fission contributions differ in the GDR resonance parameters of the strength functions, in the interpretation of the k distribution, and finally in the spin distributions. Furthermore, when using Eq. (4) rather than Eq. (3), normalized strength functions have to be used. Before comparing the theoretical predictions of Eq. (4) with experimental data the calculations were folded with the response function of the NaI detector obtained from the code EGS.[22]

IV. EXPERIMENTAL RESULTS AND DISCUSSION

A. Statistical-model calculations and γ-ray energy spectra

Figure 5 shows γ-ray energy spectra obtained in coincidence with fission fragments as well as the multiplicity gated "singles" data for beam energies of 105 and 141 MeV. All data sets show the strong, characteristic "bump" starting near $E_\gamma\sim 8-10$ MeV indicating the presence of the excited-state GDR of the compound system in competition with fission and particle evaporation. For the lower bombarding energy, the singles and coincidence γ-ray spectra are quite different in the region around 10 MeV, whereas for the higher bombarding energy both spectra are similar. This can be attributed to the angular momentum dependent influence of the fission decay on the γ-ray spectrum. The singles spectrum is a mixture of γ rays from the evaporation residue decay chain and from the fission decay chain; the coincidence spectrum contains only the γ rays from the fission decay chain. Assuming a sharp cutoff in angular momentum space, one deduces from the observed[23,24] evaporation residue (ER) and fission cross sections (f): $J_{\text{crit}}^{\text{ER}}\approx 31\hbar$ and $J_{\text{crit}}^{\text{f}}\approx 39\hbar$ from $\sigma^{\text{ER}}=416$ mb and $\sigma^{\text{f}}=248$ mb for 105 MeV, and $J_{\text{crit}}^{\text{ER}}\approx 26\hbar$ and $J_{\text{crit}}^{\text{f}}\approx 66\hbar$ from $\sigma^{\text{ER}}=220$ mb and $\sigma^{\text{f}}=1145$ mb for 141 MeV, respectively. Therefore, at 105 MeV, only a small number of the highest partial waves produce fission, while at 141 MeV fission dominates at most partial waves (see also Fig. 6).

The data of Fig. 5 were then compared to calculations using the statistical-model code CASCADE.[25,5] Since the measured γ-ray spectrum is a combination of prefission and postfission γ rays, CASCADE was extended to include the statistical decay of the excited fission fragments. This procedure is described in detail in the Appendix. The input parameters were obtained as follows: The fission barrier was taken from the rotating liquid drop model for the decay of the compound system and was adjusted to reproduce the experimental evaporation residue and fission cross sections.[23,24] (The Sierk macroscopic model[26] for the fission barrier heights also required adjustments to fit the experimental cross sections and produced nearly the same results for the γ-ray spectrum.) The level densities were parametrized differently in three energy ranges: For excitation energies $E_{\text{ex}}<10$ MeV the parametrization according to Dilg[27] was used. In the intermediate region 10 MeV $<E_{\text{ex}}<20$ MeV the level density was linearly joined to the liquid drop region. There, the same level density parameter $a=A/8$ was used for the

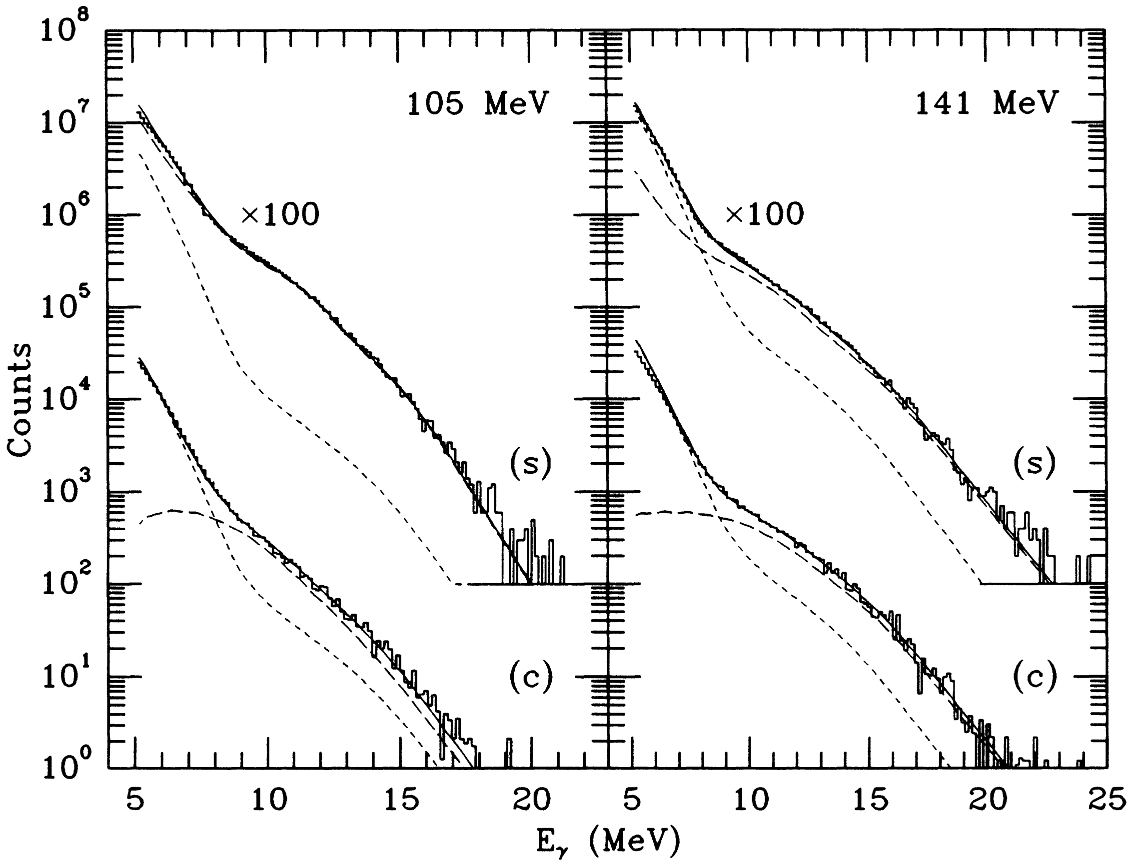

FIG. 5. Experimental γ-ray energy spectra and CASCADE calculations for 105 MeV (left) and 141 MeV (right) $^{19}F+^{181}Ta$. The "singles" data (s) are plotted in the upper parts of the figure; the coincidence data (c) in the lower parts. In the singles spectra the long-dashed curves represent the compound nucleus part including γ rays leading to residues. In the calculations for the coincidence spectra, the residue part was subtracted from the compound nucleus part yielding the prefission γ rays (long-dashed curves). The solid curves are the sum of the compound nucleus/prefission γ rays (singles/coincidence) and the postfission γ rays (short-dashed curves). The calculations were carried out with GDR parameters listed in Table I for prolate shapes.

decay of the compound system and the fission fragment decay for 105 MeV. The fission probability was computed with $a_f/a_n=1$, the ratio of level density parameters for the saddle point and equilibrium deformation. For a discussion of level density parameters for the 141 MeV data, see the following. Following the previous work[12] the GDR strength function for the compound system was taken as a double Lorentzian, and the effect of deformed fission fragments was also investigated (see Sec. IV B). The total postfission γ-ray energy spectrum included a Doppler-shift correction for coincidences with detectors $F2$ and $F4$.

CASCADE calculates the angle-integrated cross section for γ-ray emission. However, the experimental γ-ray coincidence spectrum is the average of $W(0°,E_\gamma)$ and $W(90°,E_\gamma)$, the energy dependent angular distribution with respect to the CN spin axis at 0° and 90°. With

$$W(\theta)=\tfrac{1}{3}[1+a_2^{\parallel}P_2(\cos\theta)]+\tfrac{2}{3}[1+a_2^{\perp}P_2(\cos\theta)]$$

this average can be simulated in CASCADE by effective strength values $\bar{S}^{\parallel}=\frac{3}{8}$ and $\bar{S}^{\perp}=\frac{5}{8}$ for collective prolate shapes ($\bar{S}^{\parallel}=\frac{1}{4}$ and $\bar{S}^{\perp}=\frac{3}{4}$ for noncollective oblate shapes). The coincidence γ-ray energy spectra were calculated with these strength values, whereas for the multiplicity gated "singles" γ-ray energy spectra the regular strength values of $S^{\parallel}=\frac{1}{3}$ and $S^{\perp}=\frac{2}{3}$ were taken. [Of course, the prefission and postfission γ-ray cross section entering the correlation calculation (Eq. (4)) was calculated with $S^{\parallel}=\frac{1}{3}$, $S^{\perp}=\frac{2}{3}$ since the angle dependence is explicitly included in $W(\varphi)$.] Finally, for a comparison with the data, the CASCADE calculations were folded with the response function of the NaI detector[5] and were then normalized to the data. The normalization constants involved in this procedure agree with 10%–20% with those derived from known experimental factors.

When CASCADE is applied to the coincidence data (the lower part of Fig. 5) one must be careful to follow only the decay chains leading to fission, i.e., γ rays from cascades leading to evaporation residues must be excluded. This is best done by a Monte Carlo calculation. Howev-

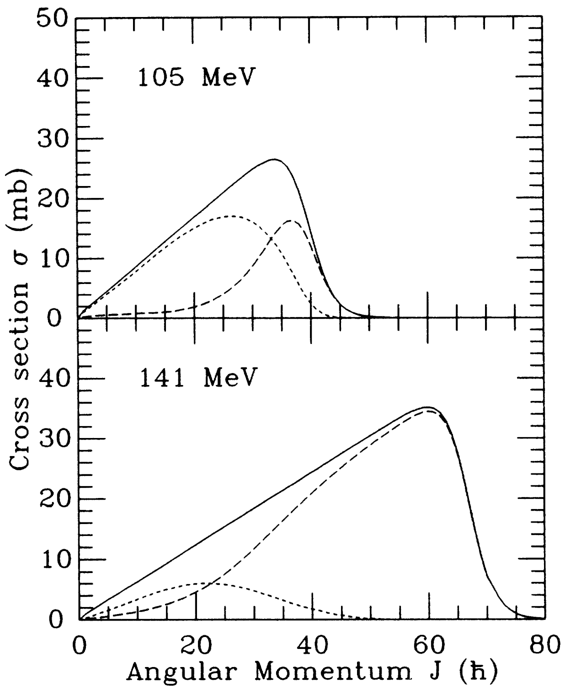

FIG. 6. Spin distribution for 105 MeV $^{19}F+^{181}Ta$ (top) and 141 MeV (bottom) calculated with CASCADE. Short-dashed curves represent the evaporation residue part, long-dashed curves the fission part. The sum of both parts gives the fusion partial cross section (solid curves).

er, a search for GDR parameters with this method is very time consuming. Thus, an alternate method was used. First, using previously measured GDR parameters[12] the relative probability for fission and residue formation was calculated with CASCADE as a function of the fusion spin (Fig. 6) using a diffuseness of $\delta J = 2\hbar$. Second, the original CN spin distribution was weighted with the residue formation probability for each spin. The resultant residue spin distribution was then used in CASCADE to calculate the γ-ray spectrum that was assumed to be associated with the decay chain leading to evaporation residues only. Subtracting this γ-ray spectrum from the CN γ-ray spectrum, calculated with the original CN spin distribution, i.e., including prefission γ rays and γ rays leading to residues, yields the prefission γ-ray spectrum. The sum of prefission and postfission γ-ray spectrum was then compared to the experimental coincidence spectrum. This subtractive procedure was checked with a full Monte Carlo calculation[28] yielding reasonable agreement.

The fits obtained with this procedure are compared to the data at 105 and 141 MeV in Fig. 5. Both the singles and the coincidence spectra for both energies are well described. This gives us confidence that the contributions of prefission and fission fragment γ rays to the total spectrum are correctly included in our formalism. The low-energy part of the coincidence spectra is dominated by the "statistical" γ rays emitted from excited fission fragments. At 141 MeV this is even true for the singles spectrum. The contribution of the γ rays from the compound system is stronger in the GDR region (>8 MeV) up to the highest measured γ-ray energies (~ 20 MeV) and thus, in this system, dominates over the fission fragment GDR which lies at a higher energy than that of the CN. Since at 105 MeV the "singles" γ rays come from a wider range of angular momenta than the coincidence γ rays, the GDR parameters at this energy were varied independently for both γ-ray energy spectra. At 141 MeV the same GDR parameters were used for the fits to the singles and coincidence data. At both energies fits were attempted for both prolate and oblate shapes of the CN. A χ^2 search for the GDR parameters, especially at 141 MeV bombarding energy, is not practical because of the extensive numerical calculations required for each decay chain. We, therefore, varied the GDR energy and width parameters in steps of ≥ 0.1 MeV and χ^2 values were calculated, for each parameter set. The final selection among fits with similar χ^2 was done by visual inspection. The resultant GDR parameters are listed in Table I. (Parameters for the fission fragment GDR are given in Sec. B.) The effect of varying the level density parameter between $A/9 \leq a \leq A/8$ is contained in the errors of the GDR parameters.

The general trend of the GDR parameters for 105 MeV can be described as follows: There is a large difference in the lower-energy GDR component for the singles and coincidence γ-ray spectra at 105 MeV result-

TABLE I. Extracted GDR parameters for ^{200}Pb from fits to the γ-ray energy spectrum. The columns contain the beam energy (MeV), the mean excitation energy (MeV) of the compound nucleus, the kind of deformation, option [whether singles (sin) or coincidence (coin) experiment], the energy and width GDR parameter for parallel and perpendicular vibrations, and the deformation parameter β, defined (Ref. 42) as $\beta=\sqrt{4\pi/5}(E^{\perp}/E^{\parallel}-1)/(E^{\perp}/2E^{\parallel}+0.8665)$.

E_{beam}	E_{ex}	Deformation	sin/coin	$E^{\parallel}$	$\Gamma^{\parallel}$	$E^{\perp}$	$\Gamma^{\perp}$	β
105	69.5	prolate	sin	11.9±0.2	3.8±0.3	15.4±0.4	5.3±0.5	0.31±0.04
			coin	10.5±0.2	7.0±0.5	15.0±0.5	9.0±0.8	0.43±0.05
		oblate	sin	16.0±0.5	3.5±0.5	12.7±0.3	5.0±0.4	−0.26±0.04
			coin	15.8±0.5	6.5±0.5	11.7±0.2	9.5±0.5	−0.33±0.04
141	102.4	prolate	sin/coin	11.5±0.3	6.5±0.4	15.8±0.5	8.5±0.5	0.38±0.05
		oblate	sin/coin	16.8±0.5	7.1±0.5	12.7±0.3	8.4±0.5	−0.31±0.04

ing in deformation parameters β which are quite different. Since the coincidence experiment at 105 MeV is sensitive to the highest partial waves only, this observation indicates a larger deformation at higher angular momenta. Both the prolate and oblate solutions describe the spectra reasonably well. The width ratio for the prolate solution is $\Gamma_{\rm high}/\Gamma_{\rm low}>1$ (oblate solution: $\Gamma_{\rm high}/\Gamma_{\rm low}<1$). The experimental systematics of the GDR built on ground states shows consistently $\Gamma_{\rm high}/\Gamma_{\rm low}>1$, a result that can also be derived from a one-body dissipation theory.[29] This suggests that at 105-MeV bombarding energy the shape of ^{200}Pb is prolate with a deformation of $\beta=0.43$ in this excitation energy-spin range. However, this statement relies on GDR systematics for deformed ground states that are available only for prolate deformed nuclei. As will be shown in the next subsection, a more definitive argument on the shape of the nucleus can be made with the help of the observed anisotropy. The GDR widths obtained from the coincidence spectra are larger than those from singles spectra. This is explained by the higher average angular momentum and mean excitation energy of the fission-coincidence GDR's.[5]

At 141 MeV, good fits were again obtained for prolate and oblate solutions (see Table I). The fact that a prolate deformation of $\beta=0.38$ or an oblate deformation of 0.31 observed at 141 MeV are comparable to the values at 105 MeV shows that the nucleus is still strongly deformed despite the significant temperature increase from 1.2 to 1.5 MeV (see the following section).

The preceding procedure that produces good fits at 105 MeV with a ratio of $a_f/a_n=1$ fails to describe the coincidence γ-ray spectrum at 141 MeV consistently. Depending on the choice of parameters one can get either a good fit to the low-energy part of the γ-ray spectrum that is dominated by the fission fragments or to the high-energy part that is dominated by the CN-GDR. It had been observed previously in a similar experiment on Thorium compound nuclei[30] that it was necessary to invoke a hindrance for fission at high excitation energies in order to obtain simultaneously a good fit in the GDR energy region and the low-energy part of the γ-ray spectrum. Such a reduction of the fission probability at high excitation energies will result in an increased split-GDR contribution from the deformed compound nucleus, and thus to a larger anisotropy in the GDR energy range (see IV B). It also enlarges the prefission neutron multiplicity, in good agreement with recent data for the compound system ^{200}Pb.[31,32] From the data of Ref. 32 there is clear evidence for such a fission hindrance at high excitation energies in the ^{19}F+^{181}Ta system, whereas for lower excitation energies (< 70 MeV) the data suggest that standard statistical-model calculations agree well with the measured prefission neutron multiplicity. These findings are in agreement with our observation that we do not need to invoke a fission hindrance at 105 MeV.

Within the present statistical-model calculations the required fission hindrance may be achieved in two ways. The first is to reduce the level density ratio a_f/a_n. Good fits were obtained with $a_f/a_n=0.94$. A reduction in the level density at the fission barrier was also investigated in Ref. 32 to describe prefission neutron multiplicities. It is difficult to understand how the level density at the fission barrier could be significantly less than that at the potential minimum. Therefore, we chose a different procedure introduced previously[30] to explain data in ^{224}Th that relates the physical process to nuclear dissipation at high excitation energies. The fission hindrance is then introduced into the statistical model by multiplying the normal fission probability $P_f(i)=\Gamma_f(i)/\Gamma_{\rm tot}(i)$ with a hindrance factor $X(i)\leq 1$, which is a free parameter in the step i of the decay chain. To preserve the total decay probability $P_{\rm tot}(i)=1$ the particle and γ-ray decay probabilities are increased proportionally. This procedure allows fission hindrance in the early steps of the decay while retaining an "unhindered" fission probability for the "cold" nucleus. To maintain agreement with the experimental fission and residue cross sections requires a further reduction of the fission barrier below the liquid drop value. Fission hindrance factors of $X(i)=0.1$, 0.1, 0.5 and $X(i)=0.2$, 0.3, 0.7 for the first, second, and third step of the decay chain, respectively, describe the coincidence γ-ray spectrum at 141 MeV equally well and show the margin of sensitivity on $X(i)$.

The effect of these fission hindrance factors on the prefission neutron mulitplicity was calculated with CASCADE along with the γ-ray spectrum. Thus, a comparison with recent neutron data of Ref. 32 offers an independent check. As in the case of the coincidence γ-ray spectrum, we subtract the calculated neutron cross section associated with evaporation residues from the total neutron cross section to obtain the prefission neutron multiplicity. The result is a prefission neutron multiplicity of $\nu_{\rm Pre}=3.3$ at 141 MeV when the fission hindrance is included. This is in good agreement with the value of $\nu_{\rm Pre}=3.7\pm0.4$ obtained at about the same bombarding energy.[32] A computation without fission hindrance produces a prefission neutron multiplicity of $\nu_{\rm Pre}=2.0$, which underlines the importance of fission hindrance.

B. Correlation data

The experimental results for the γ-ray-fission anisotropy, $W(0°,E_\gamma)/W(90°,E_\gamma)$, are presented in Fig. 7. In the region of 10–14 MeV, where the lower component of the split GDR of the deformed compound system is expected, the correlation shows a pronounced anisotropy. This establishes unambiguously that the compound system is in fact deformed. A comparison with the pattern shown in Fig. 4 indicates that either a collective prolate or a noncollective oblate shape is possible and clearly rules out a collective oblate shape. The energy region above 14 MeV, which is influenced by both the CN-GDR and the GDR of the fission fragments, shows a statistically barely significant anisotropy less than unity. This is compatible with the high-energy component of a prolate or noncollective oblate CN-GDR. Since the results from the fits to the γ-ray spectra (see Fig. 5) indicate only a minor contribution of postfission γ rays to the γ-ray spectrum in this high-energy range, the influence of a possible fission-fragment split GDR on the correlation above $E_\gamma>14$ MeV is small. However, its influence may

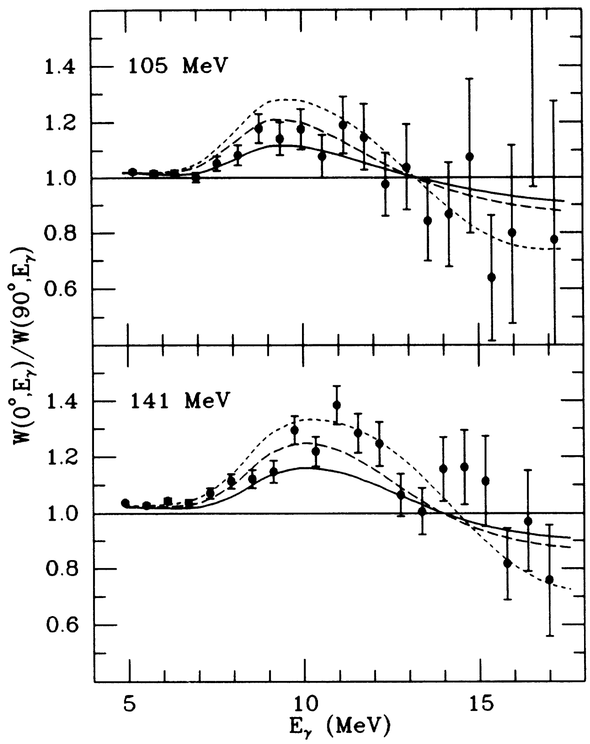

FIG. 7. Experimental anisotropies $W(0°,E_\gamma)/W(90°,E_\gamma)$ of γ-ray angular distributions with respect to the compound nucleus spin axis for 105 MeV (upper part) and 141 MeV (lower part) $^{19}F+^{181}Ta$ as a function of γ-ray energy. The solid and long-dashed curves refer to collective prolate shapes of the compound nucleus with and without thermal averaging at equilibrium deformation, respectively. Short-dashed curves correspond to noncollective oblate shapes.

be seen from the presence of $a \approx 3\%$ anisotropy for E_γ less than 6 MeV. Since this energy regime is completely dominated by postfission γ rays (see Fig. 5, bottom curves), this indicates either the presence of alignment effects in spherical fragments or emission from deformed fragments.

The curves in Fig. 7 were calculated using Eq. (4) for collective prolate shapes with and without thermal averaging at equilibrium deformation and, noncollective oblate shapes, using the best GDR parameters for the compound system previously obtained from the γ-ray spectra (Table I). We assumed prolate deformed fission fragments with GDR parameters of $E^{\parallel}$, $(E^{\perp})=14.5(16.0)$ MeV and $\Gamma^{\parallel}$, $(\Gamma^{\perp})=7.5(9.0)$ MeV and the small anisotropy at low E_γ could then be well described with a value of $K_0^{\text{frag}}=12$ to account for dealignment effects (see Sec. III). We stress the fact that these curves do not represent fits to the data but predictions for the anisotropy based on parameters obtained from the fits to the γ-ray energy spectra.

The anisotropy observed at 105 MeV is well described by the collective prolate curves. The noncollective oblate shape prediction yields too large an anisotropy at the lower component. These curves were calculated using a width of the k distribution of $K_{0,s}=8.5$ at the saddle point, and of $K_{0,\text{eq}}=15.2$ at equilibrium deformation. These values were obtained as outlined in Sec. III with the effective moment of inertia at the saddle point calculated (at the mean spin of the fission spin distribution) with the Sierk model.[26] At equilibrium deformation, the effective moment of inertia may be calculated according to[33]

$$1/\mathcal{J}_{\text{eff,eq}}=1/\mathcal{J}_{\parallel}-1/\mathcal{J}_{\perp}$$

with

$$\mathcal{J}_{\parallel}=\mathcal{J}_{sph}(1-\sqrt{5/4\pi}\beta)$$

and

$$\mathcal{J}_{\perp}=\mathcal{J}_{sph}(1+0.5\sqrt{5/4\pi}\beta)\ ,$$

where β describes the nuclear deformation at equilibrium determined by the measured GDR resonance parameters, and $\mathcal{J}_{sph}$ is the moment of inertia for rigid rotation of a spherical shape. The temperature at the saddle point for γ-fission coincidences was calculated from

$$T_s=\left[\frac{\sum_i \frac{8}{A_i}\{\langle E^i_{\text{ex}}\rangle-B^i_f-E^i_{\text{rot}}\}\sigma^i_\gamma P^i_f}{\sum_i \sigma^i_\gamma P^i_f}\right]^{1/2} \tag{5}$$

yielding $T_s=1.1$ MeV. Here, B^i_f and E^i_{rot} are the fission barrier height and rotational energy, respectively, taken at the mean spin of the population matrix of the actual decaying nucleus A_i at step i. $\langle E^i_{\text{ex}}\rangle$ is the corresponding mean excitation energy of the population matrix before γ decay of nucleus A_i minus a mean GDR energy (13.7 and 14.5 MeV at 105 and 141 MeV, respectively). At each step i the probability for fission P^i_f was calculated and σ^i_γ represents the γ-ray cross section for a GDR decay, for E_γ larger than 10 MeV. The sum over i includes all important neutron decay steps, therefore, the energy removed by prefission neutron evaporation is included in $\langle E^i_{\text{ex}}\rangle$. The temperature at equilibrium deformation was calculated from a modified Eq. (5) in which the fission barrier was not subtracted, which gives $T_{\text{eq}}=1.2$ MeV.

The extracted value of $K_{0,s}=8.5$ was then increased by three units to simulate the effect of the finite opening angle of the fission detectors. [This increased value of $K_{0,s}$ was used only in that part of the $P_s(k_s)$ distribution (see Eq. (1)) which includes the averaging over angles θ_1 and θ_2 since those k_s values directly reflect the angular acceptance range of the fission detectors; i.e., this increased value of $K_{0,s}$ was not included in the folding part of Eq. (1).] $K_{0,s}$ was varied up to a value of 14 (which is a very conservative upper limit for 105 MeV) to investigate whether the noncollective oblate solution would be able to describe the correlation data. However, even with this high value for $K_{0,s}$ the 105-MeV correlation data cannot be reproduced in the entire energy range.

To rule out a noncollective oblate shape at 105-MeV bombarding energy, the sequence of fitting the γ-ray spectrum first and then calculating the anisotropy was reversed. Assuming *a priori* a noncollective oblate shape at 105 MeV the GDR energy components $E^{\parallel}$ and $E^{\perp}$ were obtained with a χ^2 search to the anisotropy data using the formalism described in Sec. III. To allow for a practical χ^2 search the GDR width parameter for the compound nucleus were kept constant. Since no systematics exists for the GDR built on high excited states for deformed oblate shapes we have explored two different methods: First, the GDR width values were kept at equal values for the parallel and perpendicular resonance components for each search run. Second, they were allowed to differ by 2 MeV (with $\Gamma_{\mathrm{high}}/\Gamma_{\mathrm{low}} < 1$), a value that is a good compromise for GDR width values in deformed heavy nuclei at comparable temperatures. Several search runs were performed by varying the GDR width parameters between 4 and 11 MeV. (Other entries, like the prefission and postfission γ-ray contribution, the K_0 values, GDR parameter for the fission fragments were also kept fixed for each search run.) Using the CN-GDR parameter obtained with this procedure, the γ-ray energy spectrum was then calculated with CASCADE. The result can be summarized as follows: (i) The best χ^2 to the anisotropy data requires $\Gamma \approx 4-6$ MeV for the GDR widths using method 1; alternatively, a similar χ^2 was obtained with $\Gamma_{\mathrm{low}} \approx 8$ MeV, $\Gamma_{\mathrm{high}} \approx 6$ MeV using method 2. However, in either case, the associated GDR energies fail to describe the γ-ray energy spectrum, thus rejecting this solution. This is demonstrated by the solid curve in Fig. 8. (ii) A simultaneous description of the anisotropy data and the γ-ray energy spectrum required GDR widths of $\Gamma \approx 10-11$ MeV (dashed curve in Fig. 8). (However, the χ^2 for the γ-ray energy spectrum is now larger than the χ^2 obtained with the oblate parameters from Table I.) The main reason for these large width values is that enough GDR strength in the γ-ray energy spectrum around $E_\gamma \approx 9$ MeV is required. In principle, this could also be achieved by lowering the lower GDR energy component. This, however, worsens the fit to the anisotropy data considerably. These Γ values of 10–11 MeV are in clear contradiction to systematics[1,4,5] at comparable excitation energies in heavy nuclei. The only consistent description whose GDR parameter agrees with systematics is a prolate shape. Thus we conclude that ^{200}Pb has a prolate shape with a $\beta=0.43$ at an excitation energy of ~ 69 MeV, or mean GDR temperature of $T=1.2$ MeV, and angular momenta between $30\hbar$–$40\hbar$ (see Fig. 6).

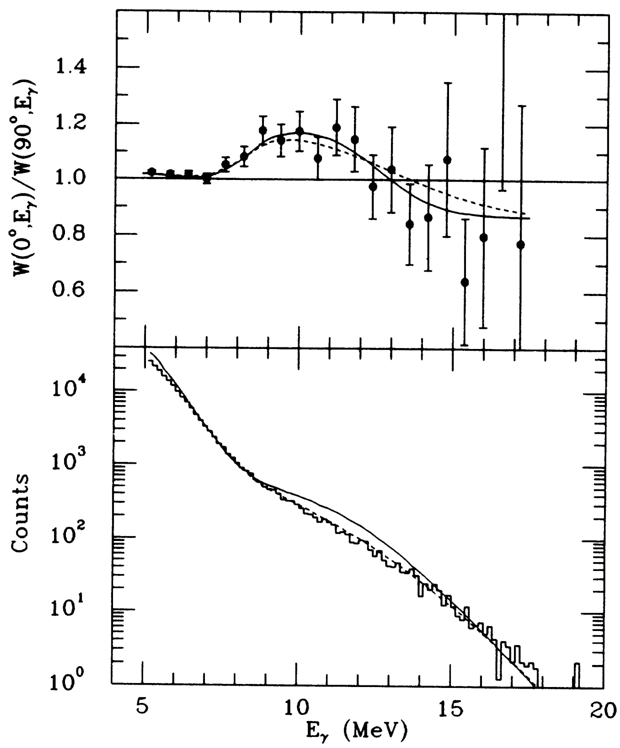

FIG. 8. Experimental anisotropies (upper part) and γ-ray energy spectrum (lower part) for 105 MeV ^{19}F+^{181}Ta. The curves represent calculations using oblate GDR parameters. The solid curves were calculated with $\Gamma=6$ MeV, $E^{\perp}=12.3$ MeV, $E^{\parallel}=13.8$ MeV; the dashed curves with $\Gamma=10$ MeV, $E^{\perp}=12.6$ MeV, $E^{\parallel}=14.8$ MeV.

Similar calculations for the anisotropy at 141 MeV do not conclusively differentiate between the collective prolate and noncollective oblate solutions. At this energy we extracted $T_s=1.4$ MeV, $T_{\mathrm{eq}}=1.5$ MeV, $K_{0,s}=10$, and $K_{0,\mathrm{eq}}=18.2$ with the same procedure as already mentioned. Even varying the value for $K_{0,s}$ within reasonable limits does not rule out completely one or the other solution, although the noncollective oblate solution seems to be favored for higher $K_{0,s}$ values.

The experimental anisotropy at 141 MeV is manifestly larger than that at 105 MeV. This could be due either to a change from a prolate to a noncollective oblate shape, or to an onset of fission hindrance in a still prolate deformed compound system. This is because a reduction of the nearly isotropic postfission γ rays increases the net anisotropy. The calculated curves at 141 MeV in Fig. 7 already include the hindrance factors that were needed to fit the γ spectra. Still, the data exceed the prolate solution at its maximum.

Dudek and Werner[14] have computed the potential energy surface of ^{200}Pb as a function of angular momentum and temperature. At $J=40\hbar$ they obtain a prolate superdeformed minimum in ^{200}Pb at $\beta=0.5$ and a noncollective oblate minimum at $\beta=0.2$, at zero temperature. At a temperature of 1.1 MeV and spin $J=40\hbar$ the calculation predicts a prolate superdeformed minimum around $\beta \approx 0.5$, which eventually will be washed out at temperatures larger than $T=1.3$ MeV resulting in a broad minimum at a small noncollective oblate deformation of $\beta \approx 0.05$. For even higher spins ($J=80\hbar$) the calculations predict a prolate hyperdeformed minimum. In this experiment the average GDR temperature changes from 1.2 to 1.5 MeV with mean spins for the fission coincidences of $\langle l \rangle^f=34\hbar$ and $\langle l \rangle^f=50\hbar$ for 105 and 141 MeV, respectively. This data would be consistent with a transition from collective prolate to a noncollective oblate shape between $T=1.2$ and 1.5 MeV, but the extracted oblate deformation of $\beta=0.31$ is much larger than expected.

Recently, the possibility of statistical fluctuations around the equilibrium shape were considered[3,34,35] and their effects on experimental γ-ray angular distributions, measured with respect to the beam axis, were discussed.[7] We investigated to what extent shape fluctuations can influence the anisotropy $W(0°,E_\gamma)/W(90°,E_\gamma)$ using the potential energy surface calculation from Dudek and Werner. The free-energy matrix $\mathcal{F}(\beta,\gamma)$ as a function of deformation parameters β and γ was obtained in steps of 0.05 in β and 5° in γ at a temperature of 1.1 MeV and angular momentum of $40\hbar$ (these values compare to the respective mean values at 105-MeV bombarding energy). The angular distribution was calculated as

$$W(\theta,E_\gamma,\beta,\gamma)=1+a_2(E_\gamma,\beta,\gamma)P_2(\cos\theta) ,$$

where the a_2 coefficient as a function of deformation parameters β and γ is given by

$$a_2(E_\gamma,\beta,\gamma)=a_{2,x}F_x(E_\gamma,\beta,\gamma)+a_{2,y}F_y(E_\gamma,\beta,\gamma)+a_{2,z}F_z(E_\gamma,\beta,\gamma)$$

with $a_{2,x}=-1$ (GDR vibration along spin axis) and $a_{2,y}=a_{2,z}=\frac{1}{2}$ (vibration perpendicular to spin axis). The normalized GDR strength function is denoted by F_i with

$$f_i(E_\gamma,\beta,\gamma)=S_i\frac{\Gamma_i E_\gamma^4}{[E_\gamma^2-E_i^2(\beta,\gamma)]^2+(\Gamma_i E_\gamma)^2} ,$$

$$F_i(E_\gamma,\beta,\gamma)=f_i(E_\gamma,\beta,\gamma)\Big/\sum_{j=x,y,z} f_j(E_\gamma,\beta,\gamma) .$$

Here, the GDR resonance energies E_i were taken to be inversely proportional to the nuclear radius, $E_i \propto 1/R_i$ with $R_i=R_0(1+\delta R_i)$. The proportional constant was chosen as such to ensure volume conservation and $S_i=\frac{1}{3}$ for $i=x,y,z$. The change in radius for triaxial shapes, δR_i, was computed as[33]

$$\delta R_i=\left[\frac{5}{4\pi}\right]^{1/2}\beta\cos\left[\gamma-i\frac{2\pi}{3}\right] .$$

[The convention is such that $\gamma=-60°$ refers to noncollective oblate (symmetry axis along x direction), $\gamma=0°$ refers to collective prolate (symmetry axis along z direction), and $\gamma=60°$ refers to collective oblate (symmetry axis along y direction).]

Finally, the ratio $W(0°,E_\gamma)/W(90°,E_\gamma)$ including shape fluctuations was calculated as[13]

$$\left\langle\frac{W(0°,E_\gamma)}{W(90°,E_\gamma)}\right\rangle=\frac{\int[W(0°,E_\gamma,\beta,\gamma)/W(90°,E_\gamma,\beta,\gamma)]\exp[-\mathcal{F}(\beta,\gamma)/T]\beta d\beta\, d\gamma}{\int\exp[-\mathcal{F}(\beta,\gamma)/T]\beta d\beta\, d\gamma}$$

for $T=1.1$ MeV and $J=40\hbar$. Figure 9 shows the influence of shape fluctuations on the anisotropy compared to a calculation that does not include those fluctuations. For simplicity, the contribution of γ rays emitted from fission fragments and all attenuation effects were neglected. Clearly, the fluctuations do not wash out the pronounced anisotropy, but manifest the expected highly deformed nature of ^{200}Pb at temperatures around 1 MeV.

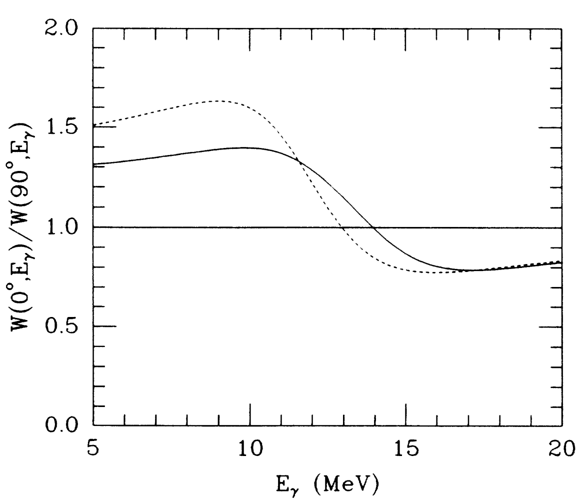

FIG. 9. Calculated anisotropies for the GDR decay of the compound system ^{200}Pb. The solid curve includes the effect of shape fluctuations at $T=1.1$ MeV and $J=40\hbar$ using a constant GDR width of $\Gamma=5$ MeV. For comparison, the dashed curve shows a calculation without fluctuations using prolate GDR parameters of $E^{\parallel}=10.5$ MeV, $E^{\perp}=15$ MeV, and $\Gamma=5$ MeV.

We note that, so far, shape fluctuations have always been treated in the context of constant temperature rather than constant excitation energy. Obviously, this needs to be improved. In addition, there is the question how to treat a thermal averaging of orientations for triaxial shapes that are being explored by shape fluctuations, and for which the k projection of the total angular momentum is not a good quantum number.

V. CONCLUSIONS

This experiment demonstrates that the angular correlation between GDR γ rays and fission fragments is a sensitive indicator of a deformed compound nucleus. The correlation can be quantitatively translated into the correlation between γ rays and the CN spin axis. Thus it can be used to differentiate between the various oblate and prolate shapes which was not possible from fits to the γ-ray spectra alone.

Our results on the correlation in the ^{19}F+^{181}Ta fusion reaction confirm the previous report[12] of a large deformation in neutron deficient Pb isotopes at excitation energies from 69.5 to 102.4 MeV. The correlation determines the shape as prolate at excitation energies of ~ 69 MeV but cannot distinguish between a collective prolate or noncollective oblate shape at ~102-MeV excitation energy. At 105 MeV a deformation of β=0.43 was measured in a narrow high spin range associated with fission. This deformation decreases to $\beta=0.38$ (for a prolate solution) at 141 MeV, where the experiment samples a much wider spin range.

The 105 MeV data alone show a spin dependent evolution of deformation: The singles data that average over the whole spin range produce a deformation of $\beta=0.31\pm0.04$. It was shown before[15] that these data could be described by a spherical shape at angular momenta below $L_{\rm crit}=16\hbar$, and a two-Lorentzian strength function above $L_{\rm crit}$, yielding $\beta=0.37\pm0.04$. The coincidence requirement selects even higher spins (the fission cross section is large for $L>30\hbar$) resulting in a much larger deformation, $\beta=0.43\pm0.05$.

This experiment proves that ^{200}Pb, which is nearly spherical in its ground state, has a superdeformed prolate shape at 69.5-MeV excitation energy and angular momentum $L>16\hbar$. We note that the presence of superdeformation in nuclei with $A\approx200$ has since been confirmed by discrete γ-ray spectroscopy in Hg isotopes.[36] The $\beta=0.43$ observed in our experiment agrees well with the $\beta\approx0.5$ of the discrete band when the higher temperature ($T=1.2$ MeV) of our experiment is considered. The phase transition to a noncollective oblate shape, which is predicted in a temperature range between 1.3 to 1.5 MeV by the basic model, cannot be ruled out by our data. One expects a noncollective oblate deformation to have a small β and this is borne out by the cranked-shell-model calculations.[14] However, this data yields large β values over the entire temperature range.

Finally, the analysis of the 141-MeV data requires a reduced fission probability compared to lower excitation energies, consistent with recently measured prefission neutron multiplicities. Thus, GDR γ-ray-fission angular correlations are also useful for the study of the fission dynamics at high temperatures in very heavy systems.

ACKNOWLEDGMENTS

We are grateful to J. Dudek and T. Werner for providing us with results from their cranked-shell-model calculation for ^{198,200,202}Pb nuclei, and wish to thank P. Bond for helpful discussions. This research was supported in part by the National Science Foundation. One of us (R.B.) acknowledges the support of the Deutsche Forschungsgemeinschaft, Bonn, West Germany.

APPENDIX: MODIFICATION OF CASCADE

The statistical-model code CASCADE (Ref. 25) was extended to include the statistical decay of fission fragments following compound nucleus fission. This was achieved by calculating the necessary details such as fission fragment excitation energies E_f^* and spins J_f, needed for the complete fission fragment decay, along with the calculation of the CN decay.

In order to handle the fission fragment decay as realistically as possible, a mass distribution for each fissioning nucleus was included. Values for the width of the mass distribution were taken from measurements in similar heavy-ion systems,[37,38] which give $\Gamma^{\rm FWHM}=30$ and 35, for 105 and 141 MeV, respectively. The fragment charge number Z_f for a given fragment mass A_f was obtained from the assumption of equal charge displacement,[20] which means that the difference between the most probable fragment charge and the charge of the most stable isobar $Z_{\rm stable}$ of a particular mass chain is the same for the light and heavy fragments: $(Z_f-Z_{\rm stable})_{\rm light}=(Z_f-Z_{\rm stable})_{\rm heavy}$. The charge of the most stable isobar for both fission fragments was calculated from Green's formula[39] describing the valley of β stable nuclei: $N-Z_{\rm stable}=0.4A_f^2/(200+A_f)$. It turned out that the fragment charge number had a strong influence on the low-energy part of the γ-ray spectrum.

During the "normal" compound nucleus CASCADE calculation, the population matrix $\sigma^f(E_f^*,J_f)$ for each fission fragment was created from a given excitation energy $E^*_{\rm nucl}$ and spin $J_{\rm nucl}$ of each fissioning nucleus. For simplicity, the mass differential cross section $d\sigma^f/dA_f$ was assumed to be the same for all masses. The total excitation energy for both fission fragments is shared according to their mass yielding the excitation energy for each fragment

$$E_f^*=\frac{A_f}{A_{\rm nucl}}(E^*_{\rm nucl}+Q^f-\langle E_k\rangle)\ ,$$

where Q^f is the Q value for fission calculated from the binding energies of the fission fragments minus the binding energy of the fissioning nucleus, and $\langle E_k\rangle$ is the total mean kinetic energy of both fragments. The latter was assumed to have a Gaussian distribution with a mean value given by the Viola systematic[40] and a FWHM taken from experiment[37] (FWHM=22 and 25 MeV for 105 and 141 MeV, respectively).

The available total angular momentum for both fragments, J_T, was parametrized from measurements[21] of the γ-ray multiplicities of the fission fragments that read for

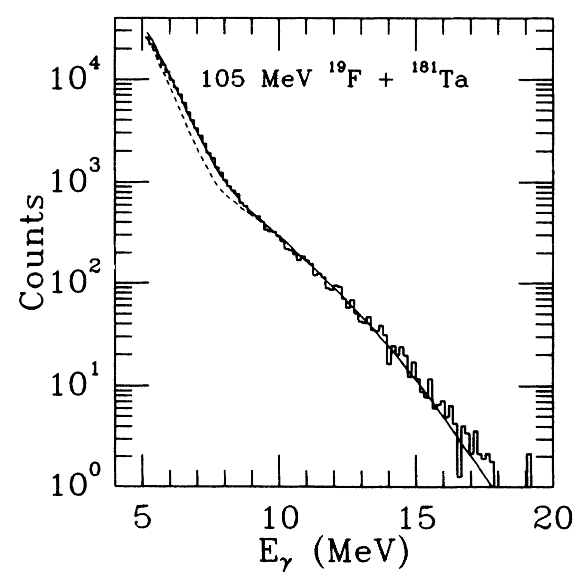

FIG. 10. Comparison of CASCADE calculations to the experimental γ-ray energy spectrum in coincidence with fission fragments for 105 MeV ^{19}F+^{181}Ta, including a fission fragment mass distribution (solid curve) and without a mass distribution (dashed curve).

symmetric fission

$$J_T = \tfrac{2}{7} J_{\rm nucl} + S(J_{\rm nucl}) ,$$

$$S(J_{\rm nucl}) = 18.0 - 0.17 J_{\rm nucl} .$$

$S(J_{\rm nucl})$ describes the deviation from a rigid rotation of two touching fragments due to statistical excitation of collective modes.[21,41] Since no dependence of the average multiplicity on the mass asymmetry was observed, within statistical errors, for the ^{19}F+^{181}Ta reaction,[41] the total spin was divided equally between both fission fragments: $J_f = J_T/2$.

At the end of the CASCADE calculation for the CN decay (yielding the prefission γ-ray spectrum) the population matrix of the first fission fragment becomes the starting point for the next CASCADE calculation of the statistical decay of that fragment. For the fission fragment CASCADE calculations new transmission coefficients were read in to account for the difference in neutron excess between fusion evaporation nuclei and fission fragments. Finally, the γ-ray spectra for each fission fragment CASCADE calculation were summed to obtain the spectrum of postfission γ rays.

The influence of the fission fragment mass distribution on the coincidence γ-ray spectra is shown in Fig. 10 for 105 MeV ^{19}F+^{181}Ta. Results assuming symmetric fission only are shown as dashed curves indicating a discrepancy in the coincidence spectrum at $E_\gamma < 10$ MeV. The same is true for the 141-MeV fits. No variation of standard statistical-model parameters was able to resolve this discrepancy. Thus, the mass (and charge) distribution for the fission fragments was introduced as outlined above and produced good fits (solid curve in Fig. 10). We note that the influence of a fission fragment mass distribution on the singles γ-ray spectrum at 105 MeV is only minor since the low-energy part of the singles γ-ray spectrum is dominated by γ rays from evaporation residues.

---

*Present address: Nuclear Physics Division, Bhabha Atomic Research Center, Bombay 400 085, India.

[1]K. A. Snover, Annu. Rev. Nucl. Part. Sci. **36**, 545 (1986), and references cited therein.

[2]Y. Alhassid, S. Levit, and J. Zingman, Phys. Rev. Lett. **57**, 539 (1986).

[3]A. L. Goodman, Phys. Rev. C **38**, 977 (1988).

[4]D. R. Chakrabarty, M. Thoennessen, S. Sen, P. Paul, R. Butsch, and M. G. Herman, Phys. Rev. C **37**, 1437 (1988).

[5]D. R. Chakrabarty, S. Sen, M. Thoennessen, N. Alamanos, P. Paul, R. Schicker, J. Stachel, and J. J. Gaardhøje, Phys. Rev. C **36**, 1886 (1987).

[6]B. Haas, D. C. Radford, F. A. Beck, T. Byrski, C. Gehringer, J. C. Merdinger, A. Nourredine, Y. Schutz, and J. P. Vivien, Phys. Lett. **120B**, 79 (1983).

[7]K. A. Snover, *Proceedings of the Texas A&M Symposium on Hot Nuclei*, edited by S. Shlomo, R.P. Schmitt, and J. B. Natowitz (World Scientific, Singapore, 1988), p. 72.

[8]A. M. Bruce, J. J. Gaardhøje, B. Herskind, R. Chapman, J. C. Lisle, F. Khazaie, J. N. Mo, and P. J. Twin, Phys. Lett. B **215**, 237 (1988).

[9]P. Thirolf, D. Habs, D. Schwalm, R. D. Fischer, and V. Metag, Nucl. Phys. **A482**, 93c (1988).

[10]W. Hennerici, V. Metag, H. J. Hennrich, R. Repnow, W. Wahl, D. Habs, K. Helmer, U. v. Helmolt, H. W. Heyng, B. Kolb, D. Pelte, D. Schwalm, R. S. Simon, and R. Albrecht, Nucl. Phys. **A396**, 329c (1983).

[11]Th. Arctaedius, Chr. Bargholtz, R. E. Ekström, K. Fransson, B. Ritzén, and P.-E. Tegnér, Nucl. Phys. **A464**, 430 (1987).

[12]D. R. Chakrabarty, M. Thoennessen, N. Alamanos, P. Paul, and S. Sen, Phys. Rev. Lett. **58**, 1092 (1987).

[13]M. Gallardo, M. Diebel, T. Døssing, and R. A. Broglia, Nucl. Phys. **A443**, 415 (1985).

[14]J. Dudek and T. Werner, private communication.

[15]M. Thoennessen, D. R. Chakrabarty, R. Butsch, M. G. Herman, P. Paul, and S. Sen, Phys. Rev. C **37**, 1762 (1988).

[16]S. Sen, D. R. Chakrabarty, P. Paul, J. Stachel, and M. Thoennessen, Nucl. Instrum. Methods A **264**, 407 (1988).

[17]H.-O. Neidel and H. Henschel, Nucl. Instrum. Methods **178**, 137 (1980).

[18]H. Frauenfelder, R. M. Steffen, S. R. de Groot, H. A. Tolhoek, and W. J. Huiskamp, in *Alpha-ray, Beta-ray and Gamma-ray Spectroscopy,* edited by K. Siegbahn (North-Holland, Amsterdam, 1968).

[19]M. E. Rose, Phys. Rev. **91**, 610 (1953).

[20]R. Vandenbosch and J. R. Huizenga, *Nuclear Fission* (Academic, New York, 1973).

[21]R. P. Schmitt, G. Mouchaty, and D. R. Haenni, Nucl. Phys. **A427**, 614 (1984).

[22]R. L. Ford and W. R. Nelson, Stanford Linear Accelerator Center Report No. 210, 1978.

[23]D. J. Hinde, J. R. Leigh, J. O. Newton, W. Galster, and S. Sie, Nucl. Phys. **A385**, 109 (1982).

[24]J. S. Forster, I. V. Mitchell, J. U. Andersen, A. S. Jensen, E. Laegsgaard, W. M. Gibbson, and K. Reichelt, Nucl. Phys. **A464**, 497 (1987).

[25]F. Pühlhofer, Nucl. Phys. **A280**, 267 (1977).

[26]A. Sierk, Phys. Rev. C **33**, 2039 (1986).

[27]W. Dilg, W. Schantl, H. Vonach, and M. Uhl, Nucl. Phys. **A217**, 269 (1973).

[28]M. G. Herman, University of Rochester, Nuclear Structure Research Laboratory, UR-NSRL-318, 1987.

[29]Y. Alhassid, *Proceedings of the Texas A&M Symposium on Hot Nuclei,* edited by S. Shlomo, R. P. Schmitt, and J. B. Natowitz (World Scientifc, Singapore, 1988), p. 95.

[30]M. Thoennessen, D. R.Chakrabarty, M. G. Herman, R. Butsch, and P. Paul, Phys. Rev. Lett. **59**, 2860 (1987).

[31]D. J. Hinde, R. J. Charity, G. S. Foote, J. R. Leigh, J. O. Newton, S. Ogaza, and A. Chatterjee, Nucl. Phys. **A452**, 550 (1986).

[32]J. O. Newton, D. J. Hinde, R. J. Charity, J. R. Leigh, J. J. M. Bokhorst, A. Chatterjee, G. S. Foote, and S. Ogaza, Nucl. Phys. **A483**, 126 (1988).

[33]A. Bohr and B. R. Mottelson, *Nuclear Structure* (Benjamin, New York, 1975), Vol. II.

[34]Y. Alhassid, B. Bush, and S. Levit, Phys. Rev. Lett. **61**, 1926 (1988).

[35]M. Gallardo, F. J. Luis, and R. A. Broglia, Phys. Lett. B **191**,

222 (1987).

[36]E. F. Moore, R. V. F. Janssens, R. R. Chasman, I. Ahmad, T. L. Khoo, F. L. H. Wolfs, D. Ye, K. B. Beard, U. Garg, M. W. Drigert, Ph. Benet, Z. W. Grabowski, and J. A. Cizewski, Phys. Rev. Lett. **63**, 360 (1989).

[37]F. Plasil, D. S. Burnett, H. C. Britt, and S. G. Thompson, Phys. Rev. **142**, 696 (1966).

[38]B. G. Glagola, B. B. Back, and R. R. Betts, Phys. Rev. C **29**, 486 (1984).

[39]A. E. S. Green, *Nuclear Physics* (McGraw Hill, New York, 1955).

[40]V. E. Viola, K. Kwiatkowski, and M. Walker, Phys. Rev. C **31**, 1550 (1985).

[41]J. R. Leigh, W. R. Phillips, J. O. Newton, G. S. Foote, D. J. Hinde, and G. D. Dracoulis, Phys. Lett. **159B**, 9 (1985).

[42]M. Danos, Nucl. Phys. **5**, 23 (1958); K. E. Löbner, M. Vetter, and V. Hönig, Nucl. Data Tables A **7**, 495 (1970).